Magnetoresistance of magnetite

2000 J. Phys.: Condens. Matter 12 13

(http://iopscience.iop.org/0953-8984/12/1/302)

J. Phys.: Condens. Matter **12** (2000) 13–28. Printed in the UK PII: S0953-8984(00)07150-2

Magnetoresistance of magnetite

M Ziese and H J Blythe

Department of Physics and Astronomy, University of Sheffield, Sheffield S3 7RH, UK

Received 23 August 1999

Abstract. The resistivity and magnetoresistance of a magnetite single crystal and Fe_3O_4 films of various thicknesses were measured in the temperature range 70 K $< T <$ 300 K and in magnetic fields in the range -1 T $\leqslant \mu_0 H \leqslant$ 1 T. The magnetoresistance depends on both current and magnetic field direction. The anisotropic magnetoresistance is determined as the difference of the magnetoresistances in longitudinal and transverse geometry. The data were analysed within a phenomenological model above the Verwey temperature. The anisotropic magnetoresistance for currents along [100] was found to show a sign change simultaneously with that of the crystalline anisotropy constant K_1. Whereas the magnetoresistance of the single crystal saturates above the anisotropy field, the Fe_3O_4 films show a significant high-field magnetoresistance depending linearly on the applied field. This behaviour was attributed to carrier transport across antiphase boundaries. A simple model was proposed that is in good qualitative agreement with the data. The single crystal shows a significant decrease of the Verwey transition in magnetic fields applied along [110]; this leads to a magnetoresistance of 70% in an external field of 1 T.

1. Introduction

Magnetite (Fe_3O_4) is a well-known ferrimagnetic spinel with a high Curie temperature of 858 K. Recently, interest in this material has been revived, since band-structure calculations indicate a half-metallic structure with a gap in the density of states of majority carriers [1, 2]. This property, in addition to the high Curie temperature, makes magnetite very attractive for room temperature applications in various spin-electronic devices, e.g. magnetic tunnelling junctions [3]. Accordingly, in recent years there has been extensive research into properties of Fe_3O_4 films [4–10]. The first tunnelling junctions with magnetite electrodes have been fabricated [11, 12]; the experimentally observed tunnelling magnetoresistance, however, is disappointingly small, casting doubt on the half-metallic nature of Fe_3O_4. Ihle and Lorenz [13] showed, in a series of theoretical studies, that short-range order persists far above the Verwey transition leading to polaron formation and band splitting. This, in turn, leads to the semiconducting behaviour of the resistivity in the temperature range between the Verwey temperature and room temperature. Below the Verwey temperature, in the charged ordered phase, transport occurs by electron hopping.

Although magnetite has been intensively studied, there are only few data available on the magnetoresistance of bulk material [14–18]. Recently there has been some work on the magnetoresistance of magnetite films [8–10, 19]. Coey *et al* [20] compared the magnetoresistances of polycrystalline films, pressed powders and a magnetite crystal and interpreted the measured differences as arising from grain-boundary scattering. This had already been indicated by Brabers as a likely explanation for the conflicting reports on the magnetoresistance found in the literature [21]. However, a comprehensive comparison

0953-8984/00/010013+16$30.00

between bulk and thin-film magnetoresistance and a more quantitative model for the high-field magnetoresistance in magnetite films is still lacking. This is an important issue, since it has been shown [22, 23] that the magnetic properties of Fe_3O_4 films deposited on MgO differ significantly from bulk properties due to the presence of antiphase boundaries. The aim of this paper is to separate intrinsic and extrinsic magnetoresistive effects in Fe_3O_4 films by comparison with bulk, to develop a model for the magnetoresistance due to antiphase boundaries in magnetite films and to investigate the resistivity behaviour near the Verwey transition.

2. Experimental details

In this work the magnetoresistances of a single crystal of magnetite and three magnetite films deposited on MgO are investigated. The crystal was cut into a cylinder ($d = 4$ mm, $h = 13$ mm) with its axis parallel to [110]. For magnetic fields applied along the cylinder axis the demagnetizing factor is $N_\parallel = 0.07$; for fields applied perpendicular to the axis the demagnetizing factor is $N_\perp = 0.465$. The resistivity was measured with the electric current along the cylinder axis and magnetic fields applied either parallel or perpendicular to the current. In the perpendicular orientation the magnetic field was along an unknown crystallographic direction. The ac susceptibility of this same crystal was measured by Skumryev *et al* [24].

Magnetite films were fabricated by pulsed laser deposition from a stoichiometric target on heated MgO (001) substrates. The substrate temperature was about 400 °C and the background pressure in the chamber was below 2×10^{-5} Torr. The film thicknesses were estimated from the deposition time to be 200 nm, 50 nm and 15 nm; the uncertainty of this estimation is about 10%. Resistivity measurements were performed with the current along [100] in applied magnetic fields along [100] and [010]. Additionally, the 200 nm thick film was measured with the current along [110] and the magnetic field applied along [110] and $[1\bar{1}0]$.

The resistivity measurements were performed in a continuous-flow cryostat using liquid nitrogen as a coolant. The samples were attached to a copper block with vacuum grease. The temperature was measured with a platinum resistance thermometer in good thermal contact with the copper block. The transverse magnetic field was generated by an electromagnet, such that both longitudinal and transverse magnetoresistances could be measured at the same temperature after a rotation of the sample holder by 90°. According to the data of Brandt *et al* [25], in longitudinal geometry a magnetic field of 1 T at 110 K leads to a temperature shift of the platinum thermometer of about 3 mK. In transverse geometry, this shift is reduced or enhanced by a factor between 0.66 and 1.16 [25]. This temperature shift is negligible in the measurements presented here. The resistivity was measured in the standard four-point geometry with silver-paste contacts. All measurements were performed in the constant-current mode with a current in the range 10 μA to 10 mA applied by a home-made current source and the voltage measured with a Keithley model 182 nanovoltmeter. The magnetization measurements were performed in a Quantum Design MPMS-5 SQUID system. Magnetic fields were applied along the cylinder axis in the case of the single crystal and in-plane along [100] in the case of the films.

3. Results

3.1. Resistivity and magnetization

The magnetization and zero-field resistivity of the single crystal and the magnetite films are shown in figure 1. The magnetization shows a sharp jump at the Verwey temperature that

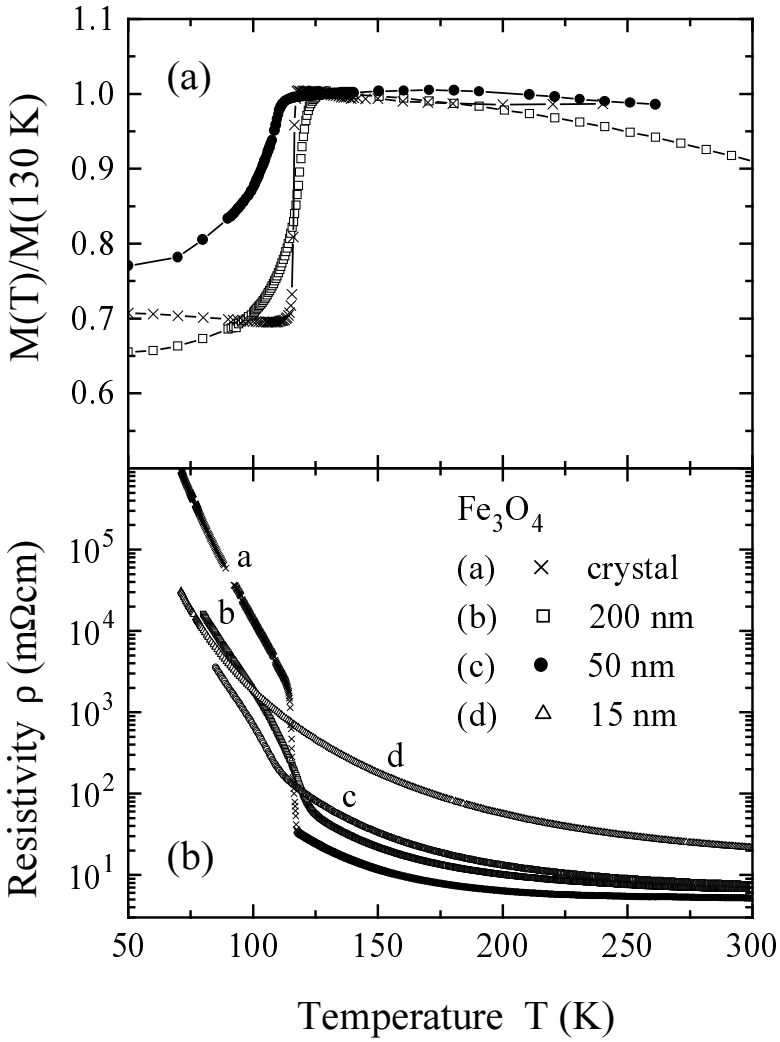

Figure 1. (a) Magnetization and (b) zero-field resistivity of a magnetite single crystal and films with thicknesses 200 nm, 50 nm and 15 nm as functions of temperature. The magnetization was measured in an applied magnetic field of 5 mT along [110] (crystal) and 0.1 T along [100] (films).

marks a structural transition from a cubic high-temperature to a monoclinic low-temperature phase. The Verwey temperature of the films decreases with decreasing film thickness in good agreement with earlier reports by Sena *et al* [7]; here we define the Verwey temperature by the maximum slope of the magnetization transition; the corresponding values are listed in table 1. The resistivity of the single crystal shows a sharp jump of about two orders of magnitude at the Verwey temperature indicating the good crystalline quality. A much broader and smaller resistivity jump can be seen for the 200 nm and 50 nm magnetite films. This is in agreement with recent reports on Fe_3O_4 films [8, 10]. The 15 nm thin film has a Verwey transition below 70 K. The Verwey temperature was determined from the maximum slope of the conductivity yielding the values listed in table 1. The Verwey temperatures determined from magnetization and resistivity measurements are in good agreement, indicating a homogeneous

Table 1. Verwey temperatures determined from magnetization and resistivity data and activation energies determined above and below the Verwey transition for the samples studied in this work.

	T_V (K)		U (meV)	
Sample	Magnetization	Resistivity	$T > T_V$	$T < T_V$
Single crystal	116.1	116.0	52	86
Film, 200 nm	118.7	118.8	56	69
Film, 50 nm	109.2	105.7	60	73
Film, 15 nm	Not measured	< 77	59	—

oxygen distribution. All samples show semiconducting behaviour below and above the Verwey transition. The activation energies U were determined from a fit of a thermally activated resistivity

$$\rho = \rho_a \exp\left[-\frac{U}{kT}\right] \tag{1}$$

to the data and are given in table 1. Whereas the high-temperature values are in agreement with values reported by Feng *et al* [19], the low-temperature values are seen to be somewhat lower than literature values [19, 26]. From the Verwey temperature of 116.1 K found for the single crystal and using the data of Shepherd *et al* [27] on the Verwey temperature shift with the non-stoichiometry parameter δ in $Fe_{3(1-\delta)}O_4$, one can infer a deviation from stoichiometry δ of about 0.0017. The high-temperature resistivity of the films is seen to increase with decreasing film thickness and is generally enhanced compared to the resistivity of the single crystal. This might indicate enhanced scattering in the films due to antiphase and grain boundaries.

3.2. Anisotropic magnetoresistance

The room temperature magnetoresistance of the Fe_3O_4 crystal and the 200 nm thick film are compared in figure 2. This figure shows the magnetoresistance ratio

$$\Delta\rho/\rho_0 \equiv [\rho(H) - \rho_0]/\rho_0 \tag{2}$$

as a function of the applied magnetic field H. ρ_0 denotes the resistivity at the coercive field, i.e. for vanishing magnetization. Within experimental error the ρ_0-values are identical in the longitudinal and transverse geometry. The measurements were performed with the current along [110] in longitudinal (solid lines) and transverse (dashed lines) geometry. For the film this corresponds to field orientations along [110] and $[1\bar{1}0]$, respectively; for the single crystal the crystallographic direction in the transverse geometry is unknown.

Both samples show a clear anisotropic magnetoresistance (AMR) with the longitudinal resistivity $\rho_\parallel$ being smaller than the transverse resistivity $\rho_\perp$. The resistivity of the crystal in the longitudinal (transverse) direction decreases (increases) and saturates to a constant value above the anisotropy field when the magnetization is aligned with the applied magnetic field. On the other hand, both the longitudinal as well as the transverse resistivity of the Fe_3O_4 film show maxima near the coercive field and decrease in higher fields. The high-field magnetoresistance seen in the film is reminiscent of the high-field magnetization slope observed in similar magnetite films on MgO [22]. Since this has been attributed to the effects of antiphase boundaries, it is likely that the high-field magnetoresistance is also due to these defects. This will be discussed in the next section. Since the high-field resistivity slopes in the longitudinal and transverse geometry are approximately equal, the anisotropic magnetoresistance defined by

$$\mathrm{AMR} = \left[\rho_\parallel - \rho_\perp\right]/\rho_0 \tag{3}$$

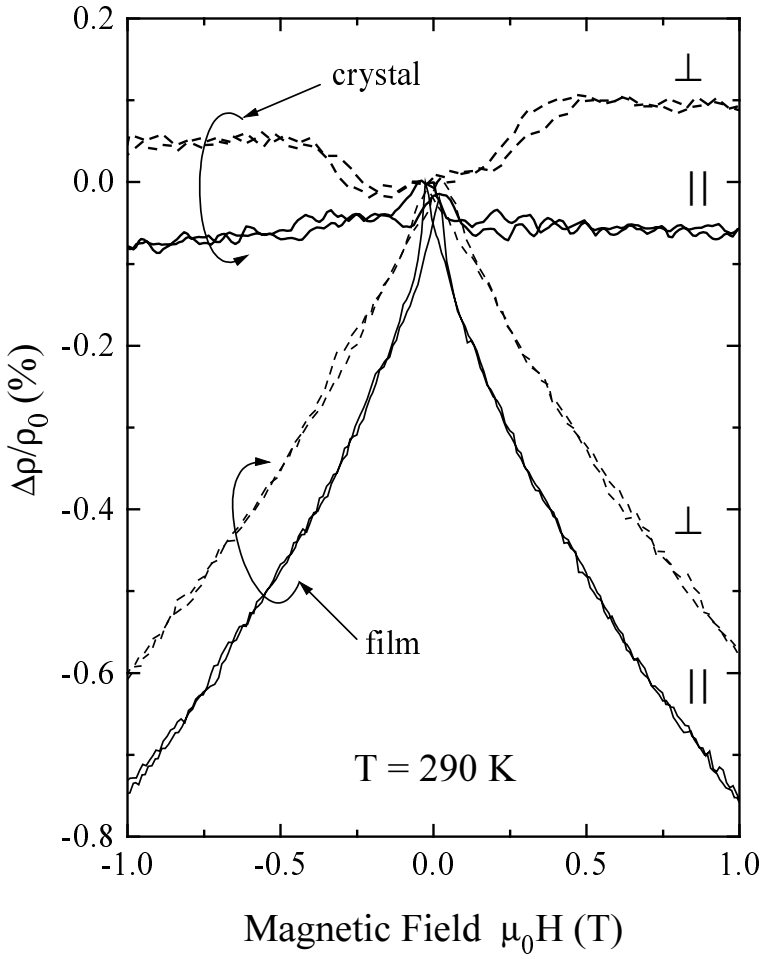

Figure 2. The magnetoresistance ratio $\Delta\rho/\rho_0$ of the Fe_3O_4 single crystal and the 200 nm thick film. The solid lines are measurements in longitudinal geometry, the dashed lines in transverse geometry. The current flow is along [110].

is field independent at high fields. This AMR will be investigated in this section.

Figure 3 shows the magnetoresistance ratio of the 200 nm thick film at 290 K and 90 K for currents along [100] and [110] in both the longitudinal and transverse geometries, respectively. These data show two interesting features of the anisotropic magnetoresistance. Firstly, the AMR depends sensitively on the current direction and secondly, the AMR has different signs at 90 K and 290 K for currents along [100], whereas it is negative at both temperatures for currents along [110].

The anisotropic magnetoresistance of the single crystal and the 200 nm thick film with a current applied along [110] determined at 1 T are shown as a function of temperature in figure 4. Above the Verwey temperature, both samples show an approximately temperature-independent anisotropic magnetoresistance ratio. In a narrow range of temperatures between 125 K and 170 K the AMR values agree. Whereas the single crystal shows a sharp AMR maximum at the Verwey temperature, the AMR values of the film are strongly reduced near the Verwey transition. In the case of the film, the AMR is small compared to the longitudinal

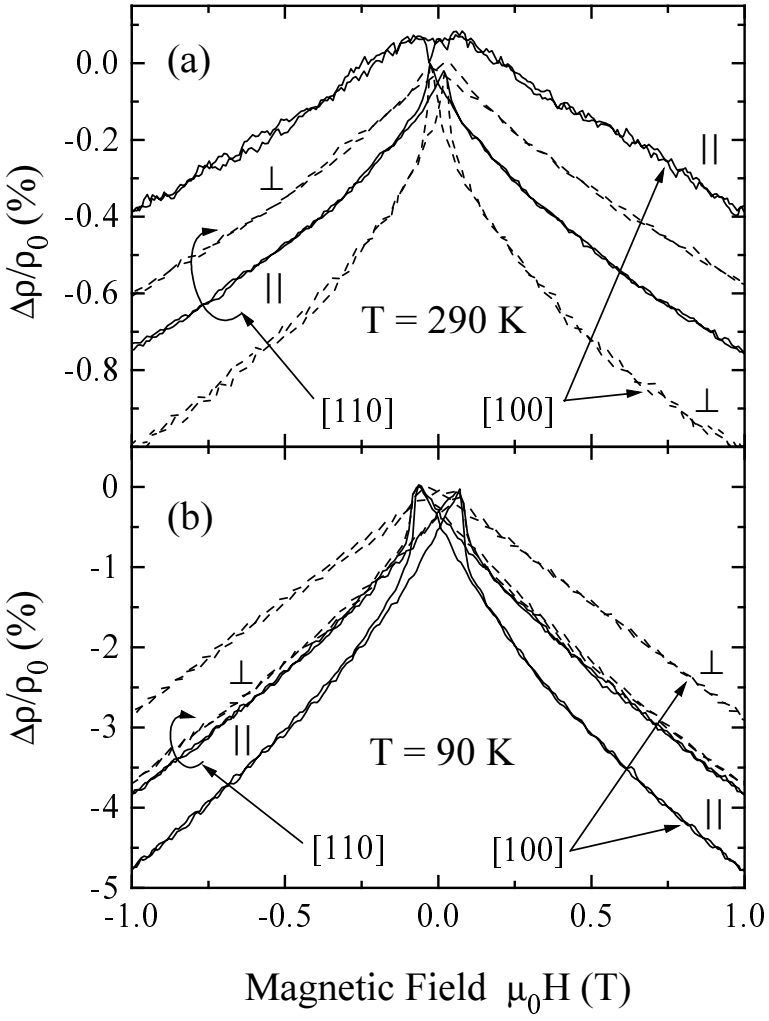

Figure 3. The magnetoresistance of the 200 nm thick Fe_3O_4 film at (a) 290 K and (b) 90 K. At both temperatures measurements with the current along [100] and [110] are compared. The magnetoresistance was measured in longitudinal (solid lines) and transverse (dashed lines) geometry.

magnetoresistance measured at 1 T (see figure 4(b)), whereas the single crystal shows only AMR at higher temperatures. Near the Verwey transition a maximum in the longitudinal magnetoresistance appears; this will be discussed in a later section. The longitudinal and transverse magnetoresistances of the film at 1 T increase by about one order of magnitude on cooling from 290 K to 90 K.

The temperature dependence of the AMR ratio for currents applied along [100] is shown in figure 5(a) for the three films investigated. Above about 180 K the AMR is approximately independent of temperature and film thickness. At lower temperatures the AMR of the thicker films changes sign. The temperature of the AMR sign change agrees with that of the sign change of the magnetic anisotropy constant K_1 [21]. Since this temperature is slightly above the Verwey temperature, it is not surprising that the 15 nm film does not show an AMR

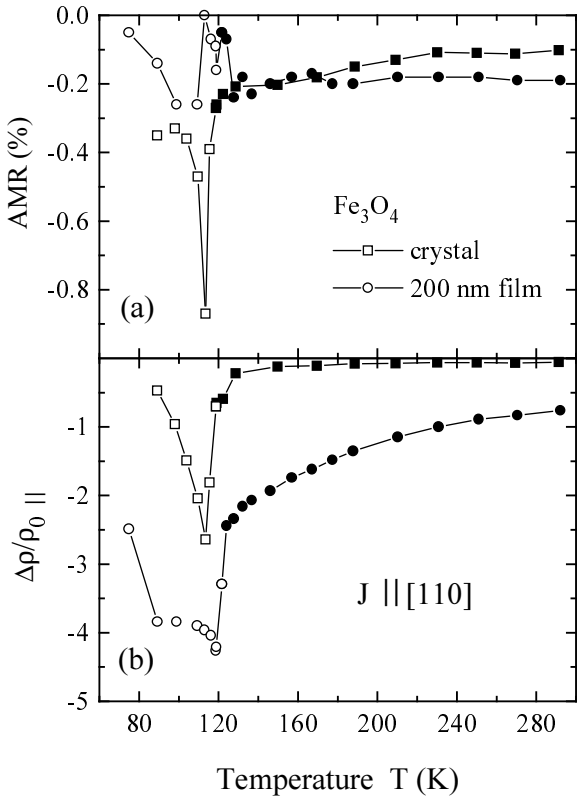

Figure 4. (a) The anisotropic magnetoresistance and (b) the longitudinal magnetoresistance at 1 T of the magnetite crystal and the 200 nm thick film as functions of temperature. The current was along [110]. Open and solid symbols indicate the monoclinic and cubic phase, respectively.

sign change in the temperature range studied $T > 70$ K. Figure 5(b) shows the longitudinal magnetoresistance of the three films for comparison.

A phenomenological description of the AMR in cubic crystals was given by Döring [28] using an expansion of the magnetoresistance of a cubic crystal in powers of the direction cosines of the magnetization ($\alpha_1\alpha_2\alpha_3$) and the electric current ($\beta_1\beta_2\beta_3$). According to Bozorth [29], using no powers of α and β higher than the second, the magnetoresistance of a cubic crystal is given by

$$\begin{aligned}\frac{\Delta\rho}{\rho_0} = {} & R_1\left[\alpha_1^2\beta_1^2 + \alpha_2^2\beta_2^2 + \alpha_3^2\beta_3^2 - 1/3\right] + 2R_2\left[\alpha_1\alpha_2\beta_1\beta_2 + \alpha_2\alpha_3\beta_2\beta_3 + \alpha_3\alpha_1\beta_3\beta_1\right] \\ & + R_3\left[s - c\right] + R_4\left[\alpha_1^4\beta_1^2 + \alpha_2^4\beta_2^2 + \alpha_3^4\beta_3^2 + 2s/3 - 1/3\right] \\ & + 2R_5\left[\alpha_1\alpha_2\beta_1\beta_2\alpha_3^2 + \alpha_2\alpha_3\beta_2\beta_3\alpha_1^2 + \alpha_3\alpha_1\beta_3\beta_1\alpha_2^2\right] \qquad (4)\end{aligned}$$

with $s = \alpha_1^2\alpha_2^2 + \alpha_2^2\alpha_3^2 + \alpha_3^2\alpha_1^2$. Although the αs appear to the fourth power, these terms can be transformed using the identity $\alpha_1^2 + \alpha_2^2 + \alpha_3^2 = 1$. The R_i are phenomenological constants. c is a numerical constant depending on the easy-axis direction. If the domains are equally distributed among the easy axes, then this constant is $c = 1/3$ for [111] easy axes ($K_1 > 0$, $K_2 > 0$ or $K_1 > -K_2/9$, $K_2 < 0$), $c = 1/4$ for [110] easy axes ($-4K_2/9 < K_1 < 0$) and $c = 0$ for [100] easy axes ($K_1 < K_2/9$, $K_2 > 0$ or $K_1 > -K_2/9$, $K_2 < 0$).

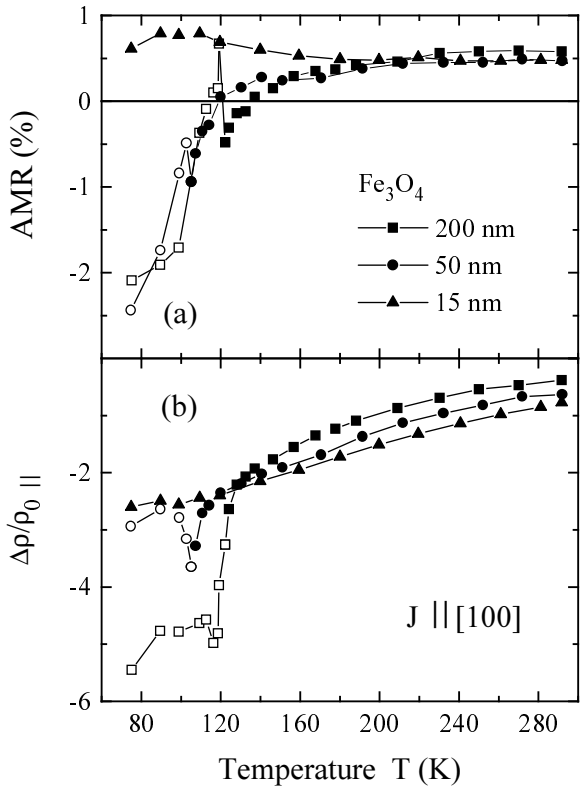

Figure 5. (a) The anisotropic magnetoresistance ratio and (b) the longitudinal magnetoresistance at 1 T for three magnetite films with 200 nm, 50 nm and 15 nm thickness. The current was along [100]. Open and solid symbols indicate the monoclinic and cubic phase, respectively.

Since the domains are unlikely to be equally distributed among the easy directions at the coercive field, which was the point used to define ρ_0, the absolute values of $\Delta\rho/\rho_0$ will not be considered for comparison with theory; the discussion will be restricted to the measured AMR values that are independent of the domain configuration near the coercive field.

For currents applied along [100], the longitudinal resistivity $(\Delta\rho/\rho_0)_\parallel$ for fields along [100], the transverse resistivity $(\Delta\rho/\rho_0)_\perp$ for fields along [010] and the anisotropic magnetoresistance are given by

$$(\Delta\rho/\rho_0)_\parallel = 2R_1/3 - cR_3 + 2R_4/3 \tag{5}$$

$$(\Delta\rho/\rho_0)_\perp = -R_1/3 - cR_3 - R_4/3 \tag{6}$$

$$\mathrm{AMR}_{[100][010]} = R_1 + R_4. \tag{7}$$

This is valid irrespective of the easy-axis direction. The measured anisotropic magnetoresistance, $\mathrm{AMR}_{[100][010]} = R_1 + R_4$, in the cubic phase is shown in figure 5(a) by the solid symbols. At temperatures above about 180 K it is temperature independent and has a value of $0.5 \pm 0.02\%$ for all three films investigated. At lower temperatures it is seen to decrease for the thicker films, eventually changing sign when the magnetocrystalline anisotropy constant K_1 changes sign. In the cubic phase the magnetocrystalline anisotropy energy is given by

$$E_K = K_0 + K_1 s + K_2\alpha_1^2\alpha_2^2\alpha_3^2. \tag{8}$$

Since R_4 is the expansion coefficient of $\Delta\rho/\rho_0$ in s and K_1 is the expansion coefficient of the free energy in s, one might speculate that R_4 is proportional to K_1 and causes the sign change of the anisotropic magnetoresistance. Then it would be likely that $R_4 \gg R_1$.

For currents applied parallel to [110], the longitudinal resistivity $(\Delta\rho/\rho_0)_\parallel$ for fields along [110], the transverse resistivity $(\Delta\rho/\rho_0)_\perp$ for fields along $[1\bar{1}0]$, the anisotropic magnetoresistance $\mathrm{AMR}_{[110][1\bar{1}0]}$ and the anisotropic magnetoresistance $\mathrm{AMR}_{[110]\phi}$ for fields in the [110] plane, i.e. along $(\cos\phi/\sqrt{2}, -\cos\phi/\sqrt{2}, \sin\phi)$, are given by

$$(\Delta\rho/\rho_0)_\parallel = R_1/6 + R_2/2 - R_3/12 + R_4/12 \tag{9}$$

$$(\Delta\rho/\rho_0)_\perp = R_1/6 - R_2/2 - R_3/12 + R_4/12 \tag{10}$$

$$\mathrm{AMR}_{[110][1\bar{1}0]} = R_2 \tag{11}$$

$$\begin{aligned}\mathrm{AMR}_{[110]\phi} = {} & \{R_1/4 + 3R_2/4 + R_3/32 + 17R_4/96 + R_5/16\} \\ & + \{-R_1/4 + R_2/4 - R_3/8 - 5R_4/24\}\cos(2\phi) \\ & + \{3R_3/32 + R_4/32 - R_5/16\}\cos(4\phi).\end{aligned} \tag{12}$$

In the case of the 200 nm thick film the transverse orientation is known and the measured anisotropic magnetoresistance in the cubic phase—see the solid symbols in figure 4(a)—is equal to R_2. Thus R_2 is seen to be temperature independent with a value of about $-0.2\pm0.02\%$. The fact that the anisotropic magnetoresistance of the single crystal is similar to that of the film indicates that the transverse magnetic field direction should be near to $[1\bar{1}0]$ ($\phi = 0$).

In insulating ferrites the anisotropy constants can usually be calculated as a sum of single-ion contributions. However, this is not possible in magnetite, since electron migration between Fe^{3+} and Fe^{2+} ions on octahedral sites was found to have a significant effect on the Fe^{2+} contribution to the anisotropy constant K_1 [30]. Indeed, the analysis of torque magnetometry data indicated that the Fe^{2+} contribution to K_1 changes sign above the Verwey temperature [31]. Thus, the sign change in K_1 from positive to negative values, observed in magnetite at about 130 K, was attributed to the gradual electron delocalization with rising temperature [32]. This interpretation might also apply to the observed sign change of the AMR. The simultaneous decrease of the Verwey transition temperature and the temperature of the AMR sign change with decreasing film thickness indicates the significance of electron hopping. A quantitative calculation of the magnetoresistance constants R_i has yet to be performed.

3.3. High-field magnetoresistance

As already discussed in the previous section, the high-field magnetoresistance seen in figure 2 is specific to magnetite films, in contrast to the bulk behaviour. However, this behaviour was also observed in polycrystalline samples of the colossal magnetoresistance manganites $La_{0.7}Ca_{0.3}MnO_3$ [33–36] where it was attributed to grain-boundary scattering. Since the Fe_3O_4 films studied here are grown epitaxially on MgO, it is unlikely that we can attribute the observed high-field magnetoresistance to grain boundaries. Since antiphase boundaries, however, are a common feature of magnetite films grown on MgO [22, 23], the high-field magnetoresistance might be related to electron transfer across these boundaries. The evolution of the longitudinal magnetoresistance with film thickness is indicated in figure 6 showing data for the three Fe_3O_4 films of thicknesses 200 nm, 50 nm and 15 nm at temperatures 290 K and 90 K. At room temperature, a systematic increase in the high-field slope is observed, whereas at 90 K, this trend is reversed and the thickest film is found to have the largest high-field slope and magnetoresistance value. This might indicate that the high-field magnetoresistance depends on both the density of antiphase boundaries and the spin polarization of the electrons, since the spin polarization is likely to increase below the Verwey transition.

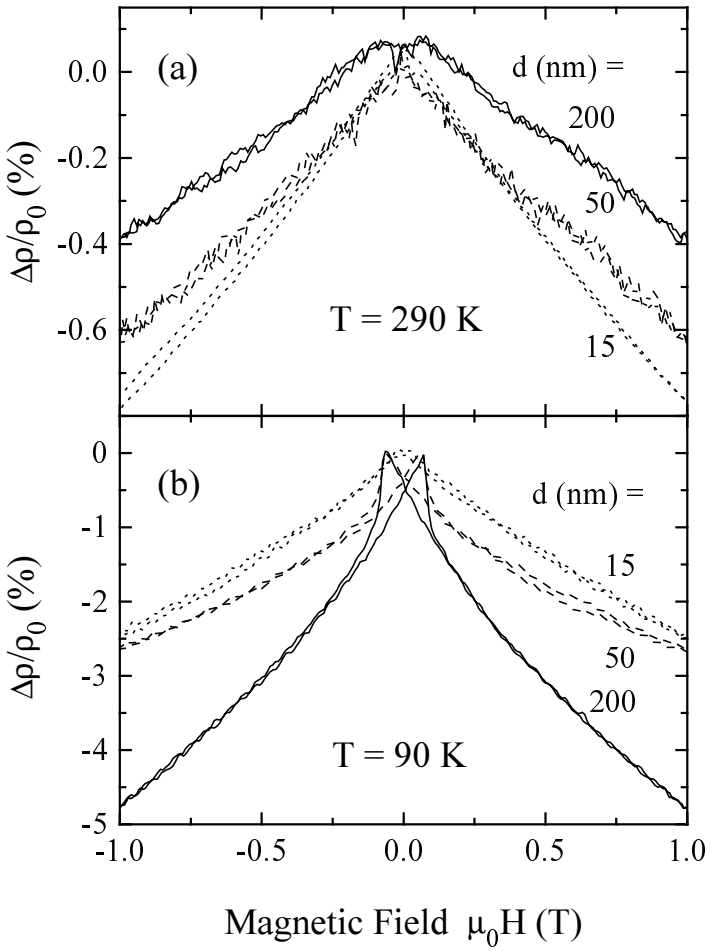

Figure 6. The longitudinal magnetoresistance of magnetite films with thickness 200 nm, 50 nm and 15 nm at temperatures of (a) 290 K and (b) 90 K.

Since the high-field magnetoresistance is approximately linear in the applied field (see figure 6) it is useful to investigate the slope

$$S \equiv \frac{\mathrm{d}}{\mathrm{d}(\mu_0 H)} \left[\frac{\Delta\rho}{\rho_0} \right] \tag{13}$$

determined at large fields. Figure 7(a) shows the temperature dependence of the slope of the high-field magnetoresistance determined in the field range 0.5 T $< \mu_0 H <$ 1 T in the longitudinal geometry. Above the Verwey transition, S is seen to decrease with temperature. In the cubic phase, the high-field slope does not depend on either current direction or magnetic field direction. This is illustrated by figure 7(b) showing the temperature dependence of S for the 200 nm thick film in transverse geometry and for two current directions, namely [100] and [110]. In the monoclinic phase a direction dependence of S is observed. This, however, does not show any clear trend and might depend on the orientation of the monoclinic axes and the twinning induced by local orientations of these axes while cooling through the Verwey transition. Although it has been deduced from torque magnetometry that the monoclinic c-axis is likely to orient along the surface normal in thick films [37], this might depend on the film

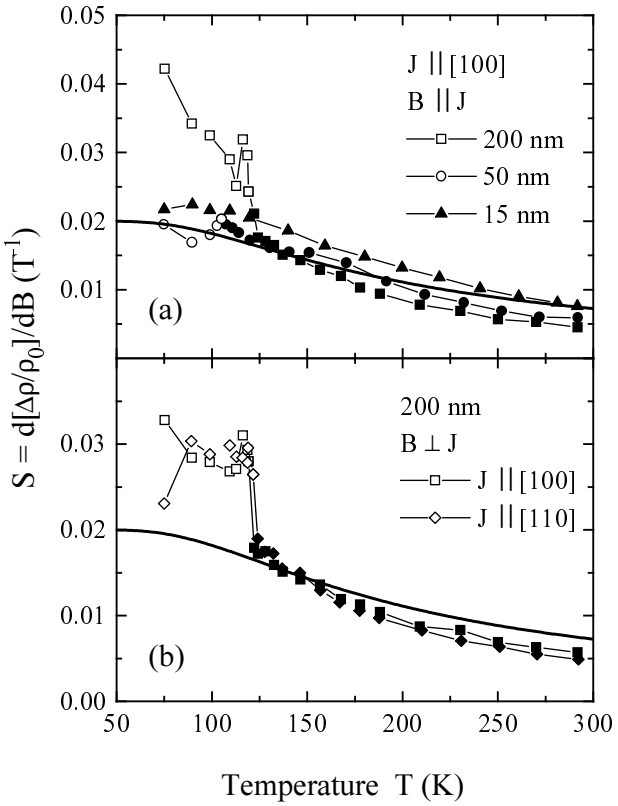

Figure 7. (a) The high-field magnetoresistance slope S of the 200 nm, 50 nm and 15 nm thick Fe_3O_4 films in longitudinal geometry for currents along [100] as a function of the temperature. The high-field magnetoresistance slope of the magnetite crystal vanishes within the experimental error, apart from in a small temperature range below the Verwey temperature. (b) The high-field magnetoresistance slope S of the 200 nm thick Fe_3O_4 film in transverse geometry for currents along [100] and [110]. The solid lines in (a) and (b) are calculated using equation (18).

thickness. Therefore, the discussion here concentrates on the cubic phase. Here the high-field slope is seen to decrease monotonically with temperature and to increase with decreasing film thickness.

Within various models it has been argued [35, 36, 38] that the high-field magnetoresistance slope in polycrystalline manganites is proportional to the grain-boundary susceptibility. Calderón *et al* [39] showed that the tunnelling conductivity through an antiferromagnetic interface in a double-exchange magnet depends linearly on the applied magnetic field in the high-field regime extending to very large fields. This relation,

$$\Delta\rho/\rho_0 \propto \chi_{apb} H \tag{14}$$

where χ_{apb} denotes the antiphase-boundary susceptibility, might also be valid for antiphase boundaries. Calculations of the antiphase-boundary susceptibility, however, have yet to be performed.

Here the following model for transport across an antiphase boundary is proposed. Consider a row of spins that, except for one spin, are ferromagnetically ordered; see figure 8. These represent the ferromagnetically ordered B-site spins within the two adjacent grains, as well as the antiferromagnetically coupled B-site spin at the antiphase boundary. This is the simplest

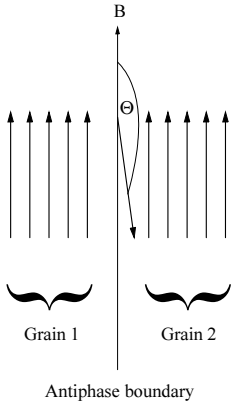

Figure 8. A schematic drawing of the antiphase-boundary model. The grains to the left and right of the antiphase boundary are assumed to have perfect ferromagnetic order. The antiphase boundary is represented by a single spin ordered mainly antiferromagnetically to the grains.

approximation for the spin configuration at the antiphase boundary which is certainly much more complex. The spins in the ferromagnetic grains are considered to be fixed along the magnetic field direction, whereas the antiphase-boundary spin is allowed to fluctuate. The energy of this spin with magnetic moment μ in an external magnetic field B is assumed to be

$$E_{apb} = \mu(B_{ex} - B)\cos\Theta \tag{15}$$

where Θ denotes the angle of the spin with respect to the applied field B and B_{ex} denotes the exchange field. Within a double-exchange model, in a classical approximation, the transfer integral is proportional to $\cos(\Phi/2)$, where Φ denotes the angle between the core spins [40]. Here $\Phi = \Theta$ and thus, the conductivity σ across the antiphase boundary is given by

$$\sigma \propto \left[\int_0^\pi \mathrm{d}\Theta\ \sin(\Theta)(1+\cos(\Theta))^2 \exp\left[-E_{apb}/kT\right]\right] \Big/ \left[\int_0^\pi \mathrm{d}\Theta\ \sin(\Theta)\exp\left[-E_{apb}/kT\right]\right]. \tag{16}$$

This yields

$$\sigma \propto \beta^{-2}\left[1+\beta+\beta^2-\beta(1+\beta)/\tanh(\beta)\right] \tag{17}$$

with $\beta = \mu(B_{ex} - B)/kT$. Since the applied field B is small compared to the exchange field B_{ex}, the conductivity is linear in magnetic field at low fields. The magnetoresistance slope is then given by $S = (\partial\sigma/\partial B)_{B=0}/\sigma_{B=0}$ yielding

$$S = \frac{2+\beta_0-\beta_0/\tanh(\beta_0)-(1+\beta_0)\beta_0^2/\sinh^2(\beta_0)}{1+\beta_0+\beta_0^2-\beta_0(1+\beta_0)/\tanh(\beta_0)}\,\frac{1}{B_{ex}} \tag{18}$$

with $\beta_0 = \mu B_{ex}/kT$. This expression contains only the parameter B_{ex}. With $\mu = 5\mu_B$, μ_B being the Bohr magneton, a reasonable agreement between data and the model can be obtained with an exchange field $B_{ex} = 100$ T; see the solid lines in figures 7(a) and 7(b). These are in qualitative agreement with the measured high-field magnetoresistance slope in the cubic phase. The model reproduces the correct magnitude of S and the experimentally observed temperature dependence, namely the decrease at higher temperatures and the saturation at lower temperatures as seen for the 15 nm thick film. The value of the exchange field is smaller than the exchange field $B_{ex} = 3kT_c/g\mu_B(S+1) = 550$ T estimated within the Weiss mean-field model with $T_c = 858$ K, gyromagnetic ratio $g = 2$ and spin $S = 5/2$. This might

be related to the simplified antiphase-boundary structure. Therefore it seems that this simple model reproduces the basic physics of carrier transport across antiphase boundaries. More realistic models should include a realistic spin configuration near the antiphase boundary as well as the interfacial spin-wave dispersion.

Within the model, the antiphase-boundary moment can be shown to be given by the modified Langevin function

$$m = \mu \left[\beta^{-1} - \tanh^{-1}(\beta)\right]. \tag{19}$$

Then the magnetoresistance slope S is not found to be proportional to the antiphase-boundary susceptibility $\partial M/\partial B$; however, S is roughly proportional to $\partial M/\partial T$.

3.4. Magnetoresistance near the Verwey temperature

The magnetoresistance of a magnetite single crystal near the Verwey transition was investigated by Gridin *et al* [18]. A sharp magnetoresistance maximum of up to 16% in a magnetic field of 7.7 T was observed at the Verwey temperature. These findings are consistent with the results of the magnetoresistance measurements performed at fixed temperature; see figures 4(b), 5(b).

In order to improve the temperature resolution, the resistivity was also recorded during temperature sweeps in various applied magnetic fields. The corresponding curves for zero field, longitudinal fields of 1.0 T and 0.3 T, and a transverse field of 1.0 T are shown in figure 9. In longitudinal fields a significant shift of the Verwey transition to lower temperatures is observed, whereas the Verwey temperature is nearly unchanged for perpendicular applied fields. The results are reproducible and do not depend on the thermal history, i.e. field-cooled cooling, field-cooled warming or zero-field cooled. The heating rate was approximately 0.3 K min^{-1}.

The magnetic induction $B = \mu_0(H + M - H_D)$ in the sample differs in the two geometries due to the different demagnetizing fields $H_D = N_{\parallel,\perp}M$. With a saturation magnetization of about 0.5 T one finds longitudinal magnetic inductions of $B_\parallel = 1.47$ T and 0.77 T corresponding to applied fields of 1 T and 0.3 T respectively, as well as a transverse magnetic induction $B_\perp = 1.27$ T corresponding to an applied field of 1 T. This excludes the possibility of an explanation of the observed differences of the Verwey temperature shift in terms of demagnetizing effects.

The longitudinal magnetoresistance ratio is shown in figure 9(b). This reaches values up to 70% in an applied field of 1.0 T, much larger than the value of about 6% reported by Gridin *et al* [18]. However, Gridin *et al* [18] measured the transverse magnetoresistance and those data are in agreement with the transverse magnetoresistance observed here. Both measurements made at constant temperature or constant field yield the same results for temperatures a few degrees from the Verwey transition. In measurements at constant temperature, the temperature was stabilized in zero field and afterwards the resistive hysteresis loop was recorded sweeping the field from 1 T to -1 T and back. For temperatures just below T_V, a large, irreversible resistance decrease was observed, when the starting field of 1 T was applied; the hysteresis loop recorded after the resistance value had settled only shows a small magnetoresistance. This might indicate that the charge-ordered state is irreversibly destroyed by a magnetic field applied in certain crystallographic directions just below T_V. On the other hand, an applied magnetic field is known to induce a switching of the c-axis in the monoclinic phase above some switching temperature; see Calhoun [26]. Therefore, the observed magnetoresistance might reflect the anisotropic conductivity in the monoclinic phase. This depends sensitively on twinning and the direction of the magnetic field that orients the c-axis. Shiozaki *et al* attributed the irregular behaviour of the Hall resistivity below T_V to c-axis switching [17]. Further investigations are necessary to clarify the magnetoresistance of Fe_3O_4 single crystals near T_V.

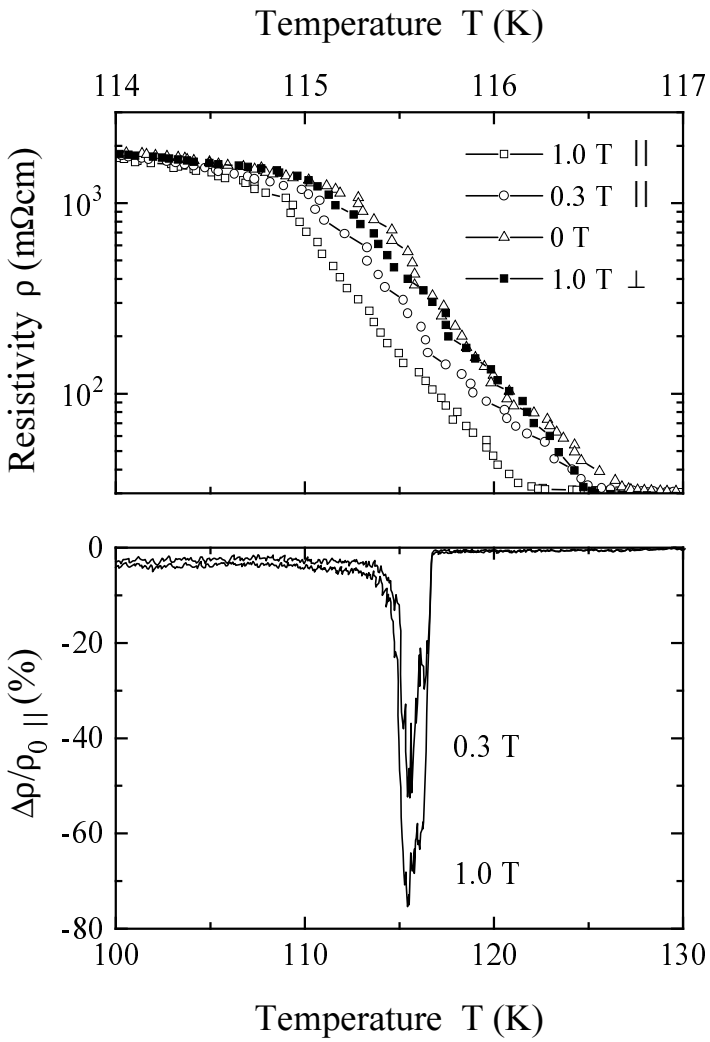

Figure 9. (a) The temperature-dependent resistivity of Fe_3O_4 single crystal in zero field, in longitudinal magnetic fields of 0.3 T and 1.0 T applied along the cylinder axis and in a transverse magnetic field of 1.0 T applied perpendicular to the cylinder axis. (b) The longitudinal magnetoresistance ratio $\Delta\rho/\rho_0$ as a function of temperature.

4. Summary and conclusions

In this work the magnetoresistance of a magnetite single crystal and epitaxial magnetite films of various thicknesses were measured and compared. The crystal and films show anisotropic magnetoresistances of the same magnitude; the AMR depends sensitively on the current and magnetic field direction. The measured AMR can be understood within a phenomenological model for the magnetoresistance in cubic crystals involving five expansion coefficients R_i, $i = 1, \ldots, 5$. Whereas R_1 and R_2 appear to be approximately temperature independent, R_4 shows a sign change simultaneously with the sign change in the anisotropy constant K_1. This is likely to be related to the gradual electron delocalization.

In contrast to the crystal, the magnetite films show a considerable, linear, high-field

magnetoresistance. This was attributed to electron transport across antiphase boundaries. A one-dimensional model was proposed that is in good qualitative agreement with the data.

The magnetite single crystal shows a large magnetoresistance of up to 70% at 1 T in longitudinal geometry near the Verwey transition. This might be attributed to a destruction of the charge-ordered state by the magnetic field or to *c*-axis switching in the monoclinic phase.

Acknowledgments

This work is being supported by the European Union TMR 'OXSEN' network. We acknowledge fruitful discussions with Gillian Gehring and Chatchai Srinitiwarawong.

References

[1] de Groot R A and Buschow K H J 1986 *J. Magn. Magn. Mater.* **54–57** 1377
[2] Pénicaud M, Siberchicot B, Sommers C B and Kübler J 1992 *J. Magn. Magn. Mater.* **103** 212
[3] Ziese M 2000 *Phil. Trans. R. Soc.* A to be published
[4] Masterson H J, Lunney J G, Coey J M D and Moukarika A 1992 *J. Magn. Magn. Mater.* **115** 155
[5] Kleint C A, Semmelhack H C, Lorenz M and Krause M K 1995 *J. Magn. Magn. Mater.* **140–144** 725
[6] Margulies D T, Parker F T, Spada F E, Goldman R S, Li J, Sinclair R and Berkowitz A E 1996 *Phys. Rev.* B **53** 9175
[7] Sena S P, Lindley R A, Blythe H J, Sauer Ch, Al-Kafarji M and Gehring G A 1997 *J. Magn. Magn. Mater.* **176** 111
[8] Gong G Q, Gupta A, Xiao G, Qian W and Dravid V P 1997 *Phys. Rev.* B **56** 5096
[9] Li X W, Gupta A, Xiao G and Gong G Q 1998 *J. Appl. Phys.* **83** 7049
[10] Ogale S B, Ghosh K, Sharma R P, Greene R L, Ramesh R and Venkatesan T 1998 *Phys. Rev.* B **57** 7823
[11] Li X W, Gupta A, Xiao G, Qian W and Dravid V P 1998 *Appl. Phys. Lett.* **73** 3282
[12] Ghosh K, Ogale S B, Pai S P, Robson M, Li E, Jin I, Dong Z-W, Greene R L, Ramesh R, Venkatesan T and Johnson M 1998 *Appl. Phys. Lett.* **73** 689
[13] Ihle D and Lorenz B 1985 *J. Phys. C: Solid State Phys.* **18** L647
Ihle D and Lorenz B 1986 *J. Phys. C: Solid State Phys.* **19** 5239
[14] Domenicali C A 1950 *Phys. Rev.* **78** 458
[15] Kostopoulos D and Alexopoulos K 1976 *J. Appl. Phys.* **47** 1714
Kostopoulos D 1972 *Phys. Status Solidi* a **9** 523
[16] Belov K P, Goryaga A N, Pronin V N and Skipetrova L A 1982 *Pis. Zh. Eksp. Teor. Fiz.* **36** 118 (Engl. Transl. 1982 *JETP Lett.* **36** 146)
Belov K P, Goryaga A N, Pronin V N and Skipetrova L A 1983 *Pis. Zh. Eksp. Teor. Fiz.* **37** 392 (Engl. Transl. 1983 *JETP Lett.* **37** 464)
[17] Shiozaki I, Hurd C M, McAlister S P, McKinnon W R and Strobel P 1981 *J. Phys. C: Solid State Phys.* **14** 4641
[18] Gridin V V, Hearne G R and Honig J M 1996 *Phys. Rev.* B **53** 15 518
[19] Feng J S-Y, Pashley R D and Nicolet M-A 1975 *J. Phys. C: Solid State Phys.* **8** 1010
[20] Coey J M D, Berkowitz A E, Balcells Ll, Putris F F and Parker F T 1998 *Appl. Phys. Lett.* **72** 734
[21] Brabers V A M 1995 *Handbook of Magnetic Materials* vol 8, ed K H J Buschow (Amsterdam: Elsevier) p 189
[22] Margulies D T, Parker F T, Rudee M L, Spada F E, Chapman J N, Aitchison P R and Berkowitz A E 1997 *Phys. Rev. Lett.* **79** 5162
[23] Voogt F C, Palstra T T M, Niesen L, Rogijanu O C, James M A and Hibma T 1998 *Phys. Rev.* B **57** R8107
[24] Skumryev V, Blythe H J, Cullen J and Coey J M D 1999 *J. Magn. Magn. Mater.* **196–196** 515
[25] Brandt B L, Rubin L G and Sample H H 1988 *Rev. Sci. Instrum.* **59** 642
[26] Calhoun B A 1954 *Phys. Rev.* **94** 1577
[27] Shepherd J P, Koenitzer J W, Aragón R, Spalek J and Honig J M 1991 *Phys. Rev.* B **43** 8461
[28] Döring W 1938 *Ann. Phys., Lpz.* **32** 259
[29] Bozorth R M 1951 *Ferromagnetism* (Princeton, NJ: van Nostrand) p 764
[30] Gerber R and Elbinger G 1970 *J. Phys. C: Solid State Phys.* **3** 1363
[31] Fletcher E J and O'Reilly W 1974 *J. Phys. C: Solid State Phys.* **7** 171
[32] Watanabe Y, Urade K and Saito S 1978 *Phys. Status Solidi* b **90** 697
[33] Hwang H Y, Cheong S-W, Ong N P and Batlogg B 1996 *Phys. Rev. Lett.* **77** 2041

[34] Gupta A, Gong G Q, Xiao G, Duncombe P R, Lecoeur P, Trouilloud P, Wang Y Y, Dravid V P and Sun J Z 1996 *Phys. Rev.* B **54** R15 629
[35] Ziese M 1999 *Phys. Rev.* B **60** R738
[36] Lee S, Hwang H Y, Shraiman B I, Ratcliff W D II and Cheong S-W 1999 *Phys. Rev. Lett.* **82** 4508
[37] Höhne R, Kleint C A, Pan A V, Ziese M and Esquinazi P 2000 *J. Magn. Magn. Mater.* to be published
[38] Evetts J E, Blamire M G, Mathur N D, Isaac S P, Teo B-S, Cohen L F and MacManus-Driscoll J L 1998 *Phil. Trans. R. Soc.* A **356** 1593
[39] Calderón M J, Brey L and Guinea F 1999 *Phys. Rev.* B **60** 6698
[40] Anderson P W and Hasegawa H 1955 *Phys. Rev.* **100** 675